



Microstructure and thermoelectric performance evaluation of p-type $(\text{Bi}, \text{Sb})_2\text{Te}_3$ materials synthesized using mechanical alloying and spark plasma sintering process

Hamta Mansouri¹, Seyed Abdolkarim Sajjadi^{1,*} , Abolfazl Babakhani¹, and Yasaman Saberi¹

¹Department of Materials Science and Engineering, Ferdowsi University of Mashhad, 9177948974 Mashhad, Iran

Received: 26 October 2020

Accepted: 25 February 2021

© The Author(s), under exclusive licence to Springer Science+Business Media, LLC, part of Springer Nature 2021

ABSTRACT

In this paper, three p-type thermoelectric compounds, namely $\text{Bi}_{0.5}\text{Sb}_{1.5}\text{Te}_3$, $\text{Bi}_{0.3}\text{Sb}_{1.7}\text{Te}_3$, and $\text{Bi}_{0.2}\text{Sb}_{1.8}\text{Te}_3$ were manufactured by mechanical milling and spark plasma sintering method. The effects of chemical composition on microstructural and thermoelectric properties were investigated. In this order, Bi, Te, and Sb powders with different contents were mechanically milled for 6 hours. Then, they were consolidated using a spark plasma sintering process (SPS) at 400 °C under 60 MPa pressure. The phase composition was analyzed using XRD with Cu-K α radiation. The microstructural characterization of the specimens was performed using scanning electron microscopy. Moreover, thermoelectric properties of the samples, including the Seebeck coefficient, electrical and thermal conductivity, power factor, and ZT were determined. Analysis of XRD patterns of fabricated compositions indicated that a single phase with a rhombohedral lattice structure was synthesized in all conditions. In addition, SEM results showed an integrated structure with a few scattered micropores. The thermoelectric results confirmed that $\text{Bi}_{0.5}\text{Sb}_{1.5}\text{Te}_3$ demonstrates the lowest thermal conductivity (0.85 W/m K), the highest electrical conductivity (4.48 S/cm), and the maximum figure of merit (1.03×10^{-2}) at room temperature. Therefore, it is the best option among the fabricated compounds to be utilized as thermoelectric materials.

Address correspondence to E-mail: sajjadi@um.ac.ir

<https://doi.org/10.1007/s10854-021-05645-8>

Published online: 13 March 2021

1 Introduction

Environmental pollution emerged from the increasing combustion of fossil fuels is a matter of global concern. Nevertheless, it provides a significant opportunity to investigate new methods to produce energy. In this regard, thermoelectric (TE) materials are introduced as a key solution. By definition, TE materials are semiconductors that can convert thermal energy to electricity and are employed in appliances such as solar cells and generators.

In recent decades, scientists have been trying to manufacture TE materials with suitable properties such as long life, no moving parts, and zero toxic gas emission [1–3]. Moreover, these materials are environmentally friendly and, thus, are good selections for exploiting wasted energy. The efficiency of TE materials is measured by a figure of merit obtained by electrons (for n-type) or holes (for p-type) and phonon conduction.

Bismuth telluride-based alloys are the best TE materials for using in the range of 300–500 K [4, 5]. The highest figure of merit of these materials was calculated at room temperature [6]. The group IV–VI compounds show good electrical transport properties, well-known semiconductors, benefit from their narrow band gap and highest figure of merit among the other thermoelectric materials at low temperatures [7, 8]. It has been reported that when thermoelectric materials are produced in the nano-sized scale, they demonstrate high thermoelectric performance [9]. The performance is evaluated using the dimensionless figure of merit, ZT which is defined as follows:

$$ZT = \left(\frac{\alpha^2 \delta}{k} \right) T, \quad (1)$$

where α is the Seebeck coefficient, δ is the electrical conductivity, k is the thermal conductivity, and T is the temperature. As it is known, in TE materials, three parameters, namely electrical conductivity, thermal conductivity, and Seebeck coefficient are determinative parameters of their performance level.

The thermal conductivity (k) includes lattice thermal conductivity (k_L) along with the electronic component (k_{el}) [10]. These semiconductor materials can obtain high-performance levels or high dimensionless figure of merit when they have high electrical conductivity, high Seebeck coefficient, and low thermal conductivity. However, due to interdependent

physical parameters in bulk samples, it is difficult to balance these three main parameters [11].

TE materials can be produced using a wide range of methods, including solvothermal [12], hydrothermal [8], melt spinning [13], microwave synthesis [14], and mechanical alloying (MA), followed by hot pressing or spark plasma sintering (SPS) [15]. The synthesis mechanism of thermoelectric material powder during ball milling includes four steps: plastic deformation, cold welding, fracture, and thermochemical reactions. The synthesized powder should be compacted and sintered to form bulk materials. There are different methods to sinter material powders. SPS is one of them. SPS is an appropriate method to prevent grain growth due to its high heating rate and short sintering time. Therefore, it can potentially attract researchers [16–20]. In specific, bismuth telluride antimony compounds are often synthesized using this method [17].

Madavali et al. [16] fabricated p-type $(\text{Bi}_2\text{Te}_3)_x(\text{Sb}_2\text{Te}_3)_{1-x}$ alloys with high TE performance by mechanical alloying followed by SPS. They found that the electrical conductivity increases with Sb content. Moreover, the $\text{Bi}_{0.3}\text{Sb}_{1.7}\text{Te}_3$ compound presented a ZT of 1.3 ± 0.06 at 400 K and 1.07 ± 0.06 at 300 K. This enhanced ZT was gained by increasing the Sb content. It was because of the increased carrier concentration and band gap of these samples.

Cho et al. [18] fabricated the $\text{Bi}_{0.5}\text{Sb}_{1.5}\text{Te}_3$ compound using SPS in the temperature ranging of 250 °C to 350 °C and investigated the microstructure and thermoelectric properties of this compound. As reported in their study, the highest figure of merit of 3.5×10^{-3} was obtained for this compound when it was sintered at 350 °C for 2 min using hydrogen-reduced powders.

Li et al. [19] manufactured the $\text{Bi}_{0.5}\text{Sb}_{1.5}\text{Te}_3$ compound using mechanical alloying and SPS methods. They reported the maximum figure of Merit (0.0048/K) for sintered samples produced in the milling time of 60 h, the ratio of ball to powder of 20:1, and the milling speed of 450 rpm.

Chen et al. [20] produced single-phase $\text{Bi}_x\text{Sb}_{2-x}\text{Te}_3$ ($x = 0.2, 0.25, 0.3, 0.34, 0.38, 0.42, 0.46, \text{ and } 0.5$) alloys prepared by SPS and MA processes. According to the research, with the increasing Sb, the electrical resistivity and the Seebeck coefficient decreased. The higher thermal conductivities at low temperatures were obtained at the compositions with lower Bi

values. As a result, the maximum ZT values of 1.23 for $\text{Bi}_{0.3}\text{Sb}_{1.7}\text{Te}_3$ compound and of 0.6 for $\text{Bi}_{0.5}\text{Sb}_{1.5}\text{Te}_3$ compound were achieved at 423 K.

Fan et al. [21] manufactured p-type $\text{Bi}_{0.5}\text{Sb}_{1.5}\text{Te}_3$ thermoelectric alloys by MA and hot pressing methods. Due to the MA process performed for 12 h, $\text{Bi}_{0.5}\text{Sb}_{1.5}\text{Te}_3$ solid solution phase was formed and the amount of the solid solution phase increased with increasing the milling time. Moreover, the fine grain size remained unchanged after hot pressing. As a result, the maximum figure of merit was gained as 2.84×10^{-3} at room temperature.

According to the literature, there are some studies performed on the fabrication of $\text{Bi}_{0.5}\text{Sb}_{1.5}\text{Te}_3$ using mechanical alloying [16, 19, 20]. However, the main drawbacks of the mentioned researches are the long time as well as the high sintering temperature needed for achieving a single-phase resulting in undesired grain growth. Considering the mentioned challenges, the present work aims to decrease the processing time and sintering temperature to gain the smaller particle size and also to evaluate the effect of the chemical composition and the size of the particles on the thermoelectric properties. For that reason, in the current research, a comparative study on the effect of the chemical composition of p-type TE compounds of $\text{Bi}_{0.2}\text{Sb}_{1.8}\text{Te}_3$, $\text{Bi}_{0.3}\text{Sb}_{1.7}\text{Te}_3$, and $\text{Bi}_{0.5}\text{Sb}_{1.5}\text{Te}_3$, synthesized using mechanical alloying and SPS on the resultant microstructure and electronic/thermal transport properties was carried out. This research will be important for the development of various thermoelectric applications of this group of advanced materials.

2 Experimental procedure

2.1 Synthesis of micro–nano-powders TE materials

$\text{Bi}_{2-x}\text{Sb}_x\text{Te}_3$ ($x = 1.8, 1.7, \text{ and } 1.5$) powders were synthesized by mechanical alloying (MA) and SPS processes. For the nominal compositions in this work, pure Te (Sigma Aldrich, 99.8%), Bi (Sigma Aldrich, 99.95%), and Sb (Sigma Aldrich, 99.95%) as raw materials were used according to the stoichiometry ratios of these elements in the different compositions. The powders were mixed in stainless-steel vials using balls with diameters of 8 to 13 mm. The milling was carried out with ball to powder ratio of 15:1 under

argon atmosphere with a speed of 300 rpm for 6 h in a planetary ball mill (PM 2400/made in Iran).

2.2 Sintering of TE powders using SPS process

All the prepared powders were sintered in the same condition by SPS method (SPS, Dr. Sinter825). The process was performed with a heating rate of $30 \text{ }^\circ\text{C}/\text{min}$ up to $400 \text{ }^\circ\text{C}$ under 60 MPa pressure. The holding time was set to 10 min. Finally, the density of the solid-state synthesized powders was measured according to the Archimedes method.

2.3 Materials characterization

Characterization of the phases produced during mechanical milling of the raw powders was performed by X-ray diffraction (XRD) using a PANalytical X'Pert PRO Alpha-1 by Cu-K α radiation ($\lambda = 1.54 \text{ nm}$). The data were collected in the 2θ range from 20° to 55° .

Morphology of the powders was observed with a field-emission scanning electron microscope (FESEM, TESCAN MIRA30XMU) using an accelerating voltage of 10 kV with a secondary electron detector. To study the microstructure of the sintered compounds, scanning electron microscopy (SEM, Zeiss ultra 55) was utilized on the polished surface of the bulk samples. Composition of the samples was estimated by energy-dispersive X-ray spectra (EDS). Moreover, particle size of the milled powders was measured using Particle Size Analyzer, Vasco3-Cordouan.

2.4 Thermoelectric transport characterization

Thermal conductivity of the samples was determined according to

$$k = \lambda \rho C_p, \quad (2)$$

in this equation, ρ represents the density of the samples, λ is the thermal diffusivity measured by LFA (Netzsch Laser Flash Apparatus), and specific heat (C_p) was measured by DSC (Netzsch-DSC404 pegasus 214 polyma).

Thermoelectric transport parameters including Seebeck coefficient (α) and electrical conductivity (δ) were measured in the temperature range of 299 to 679 K using (ULVA-RIKO ZEM3).

3 Results and discussion

3.1 Phase and structure

Figure 1 shows X-ray diffraction patterns of $\text{Bi}_x\text{Sb}_{2-x}\text{Te}_3$ ($x = 0.5, 0.3, 0.2$) TE materials prepared by milling procedure. According to Fig. 1a, high pure $\text{Bi}_{0.5}\text{Sb}_{1.5}\text{Te}_3$ and $\text{Bi}_{0.2}\text{Sb}_{1.8}\text{Te}_3$ compositions were fabricated due to the suitable time of milling (6 h). However, it was found that six-hour milling is not enough to obtain a single phase of $\text{Bi}_{0.3}\text{Sb}_{1.7}\text{Te}_3$ (PDF#71-393) chemical composition because there are some impurities (Te(JCPDS:36-1452)) in the X-ray pattern. Kitamura et al. [22] reported that single-phase $\text{Bi}_{0.3}\text{Sb}_{1.7}\text{Te}_3$ with the best thermoelectric properties was achieved when milling time was 30 h at 110 rpm (maximum ZT = 1.01 at room temperature) [22]. XRD patterns for the two nominal compositions, i.e., $\text{Bi}_{0.5}\text{Sb}_{1.5}\text{Te}_3$ (ICDD:00-049-1713) and $\text{Bi}_{0.2}\text{Sb}_{1.8}\text{Te}_3$ (ICDD:00-049-1743), shown in Fig. 1a, confirm the rhombohedral structure of the space group $R3m$ for the materials [23]. Moreover, the

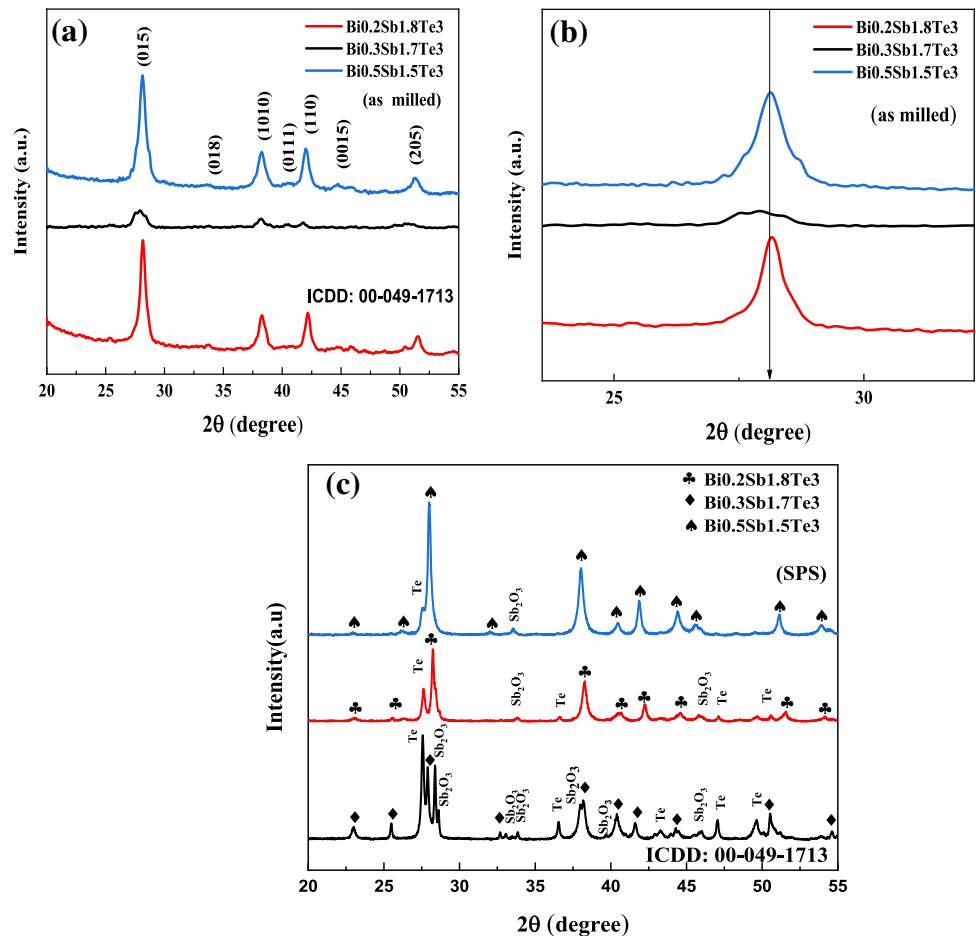
comparison between the enlarged (015) peaks of the three samples, as demonstrated in Fig. 1b, approves the presence of Sb. Substitution of Bi instead of Sb shows more intensity and d-spacing, which is because of the larger atomic radius of Bi (230 pm) compared with Sb (140 pm). Therefore, according to the Bragg equation,

$$n\lambda = 2d \sin \theta \quad (3)$$

the peaks with more Bi shift to lower angles. The diffraction peaks of samples $\text{Bi}_{0.5}\text{Sb}_{1.5}\text{Te}_3$ and $\text{Bi}_{0.2}\text{Sb}_{1.8}\text{Te}_3$ are much sharper after sintering. It means that sintering has led to better crystallinity and comparatively larger grain size due to the grain growth.

Figure 1c demonstrates the XRD pattern following sintering at 673 K for all samples. As can be seen, there are small extra peaks of Te at 27.5° in the compositions. The presence of Te in the SPSed samples can be described according to the observation of Kitamura et al. [22], in which they reported that the eutectic temperature of Te and Bi_2Te_3 is 673K.

Fig. 1 XRD pattern of: **a** as-milled powders, **b** the enlarged (015) diffraction peak of different samples, and **c** sintered alloys ($\text{Bi}_x\text{Sb}_{2-x}\text{Te}_3$ with $x = 0.5, 0.2$, and 0.3)



Certainly, Te element remained in the compositions and the heterogeneous structure have negative effects on thermoelectric properties. It should be mentioned that many investigators have reported the presence of trace amounts of some initial elements or oxides in the fabricated compounds due to the insufficient milling time, the collisions of powders with jar and balls during milling, or low vacuum in the SPS process [21, 24]. In the current study, like the above-mentioned researches, trace amounts of Sb_2O_3 and Te element in all $\text{Bi}_{0.3}\text{Sb}_{1.7}\text{Te}_3$ compounds were detected after the sintering process which may be due to the low vacuum in the SPS process. Table 1 presents the trace amounts of Sb_2O_3 and Te and the $\text{Sb}_2\text{O}_3/\text{Te}$ ratio for all the samples calculated by the area of the peaks using the Origin Software. Although, Likha et al. [25] claimed that a small enhancement in the oxygen content has not an important effect on the thermoelectric properties of materials.

3.2 Microstructure analysis

SEM morphologies of raw materials are demonstrated in Fig. 2 along with EDS analysis. As can be seen, the raw materials are multi-dimensional with rough surfaces and particle size smaller than $150\ \mu\text{m}$. In addition, according to the figure and the relevant EDS analysis, the raw materials include some oxygen. Moreover, Fig. 2a demonstrates Bi as regions with silver and white colors, while the created oxide as an iridescent sheen. Due to oxidation that sticks some particles together, some of them are bigger compared with others. The morphology of Sb and Te powders and their composition analysis can be seen in Fig. 2b and c, respectively.

Figure 3 illustrates SEM images of $\text{Bi}_{2-x}\text{Sb}_x\text{Te}_3$ ($x = 1.8, 1.7, 1.5$) milled powders. Based on the figure, an increase in the Bi content up to 0.5 at.% leads to the reduction of particle size and the uniform size distribution of powders. Specially, it can be seen that a rise in Bi content from 0.3 to 0.5 at.% results in the smaller particle size and homogenous distribution. Sb atoms, against Bi atoms, could diffuse in a conductor

due to a highly effective charge for electromigration-induced atomic diffusion. Therefore, the weak electromigration behavior of Bi atoms compared with Sb atoms leads to the lattice strain during the milling process. It means that the microstructural strain causes the fracture of powders. Hence, the refinement of particles and uniform size distribution of $\text{Bi}_{0.5}\text{Sb}_{1.5}\text{Te}_3$ alloy powders during the milling process occur [26]. The results of the particle size analysis of the synthesized powders showed that the average particle size of the $\text{Bi}_{0.5}\text{Sb}_{1.5}\text{Te}_3$ sample is smaller than the others. The mean particle size of $\text{Bi}_{0.5}\text{Sb}_{1.5}\text{Te}_3$, $\text{Bi}_{0.3}\text{Sb}_{1.7}\text{Te}_3$, and $\text{Bi}_{0.2}\text{Sb}_{1.8}\text{Te}_3$ was 23.15 nm, 24.58 nm, and 26.07 nm, respectively.

It is worth noting that an increase in the Sb-to-Bi ratio in $\text{Bi}_x\text{Sb}_{2x}\text{Te}_3$ causes increasing Sb_{Te} defects as a result, the carrier density increases which in turn, electrical resistance reduces. Moreover, diffusion of atoms can occur in a conductor under a high-density electric current, which is named electromigration. Sb atoms with a high effective charge ($140e$) and susceptible to electromigration are the suitable choices for atomic diffusion [16, 17].

Table 2 presents the chemical composition of the samples determined by EDS results. The obtained values show that all samples have Bi:Te:Sb ratio confirming the near-stoichiometric and homogenous composition. It means that the milling procedure successfully distributes the elements in $\text{Bi}_{2-x}\text{Sb}_x\text{Te}_3$ ($x = 1.8, 1.7, 1.5$) TE alloys.

Figure 4 indicates grain size distribution of $\text{Bi}_{0.2}\text{Sb}_{1.8}\text{Te}_3$, $\text{Bi}_{0.3}\text{Sb}_{1.7}\text{Te}_3$, and $\text{Bi}_{0.5}\text{Sb}_{1.5}\text{Te}_3$ -sintered samples. The grain size of the sintered bulk samples was measured by Digimizer software using SEM microstructures. The results showed that the mean grain size of bulk $\text{Bi}_{0.2}\text{Sb}_{1.8}\text{Te}_3$, $\text{Bi}_{0.3}\text{Sb}_{1.7}\text{Te}_3$, and $\text{Bi}_{0.5}\text{Sb}_{1.5}\text{Te}_3$ samples is 165, 155, and 150 nm, respectively, indicating that with an increase in Bi content, the average particle size decreases. Moreover, it can be attributed to the initial particle size of the synthesized materials after the milling process and before SPS.

Table 1 $\text{Sb}_2\text{O}_3/\text{Te}$ ratio of the different compounds calculated by the area of the peaks using the Origin Software

Compounds	Peak area of Sb_2O_3	Peak area of Te	$\text{Sb}_2\text{O}_3/\text{Te}$ ratio
$\text{Bi}_{0.2}\text{Sb}_{1.8}\text{Te}_3$	49.57	148.81	0.33
$\text{Bi}_{0.3}\text{Sb}_{1.7}\text{Te}_3$	318.26	856.7	0.37
$\text{Bi}_{0.5}\text{Sb}_{1.5}\text{Te}_3$	18.12	103.81	0.17

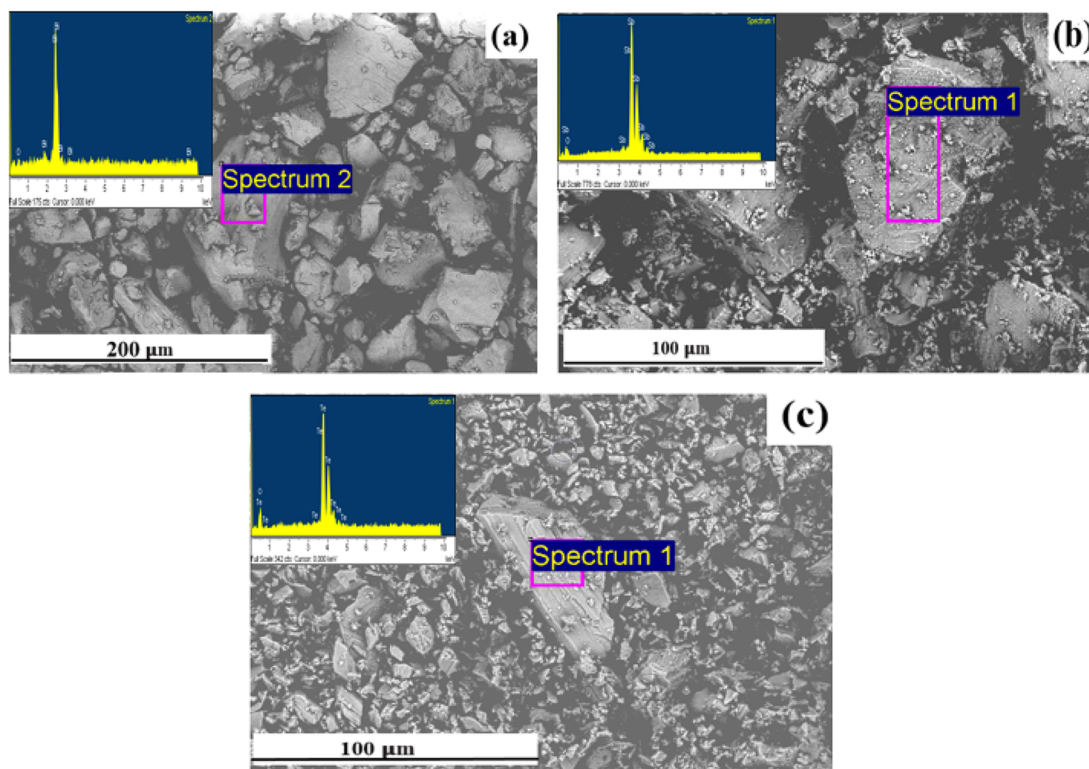


Fig. 2 Morphologies of the raw materials: **a** Bi, **b** Sb, and **c** Te powder with EDS spectrums

Li et al. [19] found that particle size decreases and particle distribution becomes more uniform with increasing milling time. As a result, the minimum particle size of 300–800 nm could be reached. They showed that after ball milling at 500 rpm for 18 h, the particle size reduces to about 100 nm; however, the particle size increases by the annealing process of sintered samples at 300 °C for 2 h [19]. In comparison with the work of Li et al. [19], the particle size obtained in the current study is smaller. Therefore, developed thermoelectric properties are expected.

Fracture surfaces of the sintered samples in the SPS condition of 400 °C/60 MPa are shown in Fig. 5. As can be seen, the grain size of the samples increases following the SPS process due to the high-temperature sintering [10].

According to Fig. 5, all samples show dense structures with some sub-micron voids, which are effective in thermoelectric properties. It is worth noting that sub-micron pores can affect the electron/hole transformation and scattering and also thermal conductivity and, thus, thermoelectric properties of the material. According to SEM images, the average pore size in the $\text{Bi}_{0.3}\text{Sb}_{1.7}\text{Te}_3$ sample is bigger than the average pore size in the other samples.

Pakdel et al. [27] found that the addition of Sb_2O_3 nanoparticles (0, 1, 4, and 6 wt.%) leads to the dispersion at grain boundaries as Zenner pinning particles. Moreover, these nanoparticles are dispersed in the matrix as pinning sites. According to the research, the SEM image shown in Fig. 5, consists of Sb_2O_3 compound introduced as white particles. The existence of Sb_2O_3 compound has been confirmed by XRD pattern presented in Fig. 1c.

Density measurement of SPS-sintered samples shows that the experimental density of the samples is in the range of 78–80% of their theoretical density; therefore, 20–22% porosity could be present in the samples. The average pore size of the samples was measured less than 1 μm. It should be mentioned that the small particle size of milled powders of the higher Bi content sample has increased its compressibility and sinterability and led to the minimum pore size.

As mentioned above, the porous structure maintains the heat in the pores and decreases the thermal conductivity. Following the sintering process, grain growth is observed; however, since sintering time in SPS is shorter than other sintering processes, it is not observed too much [28].

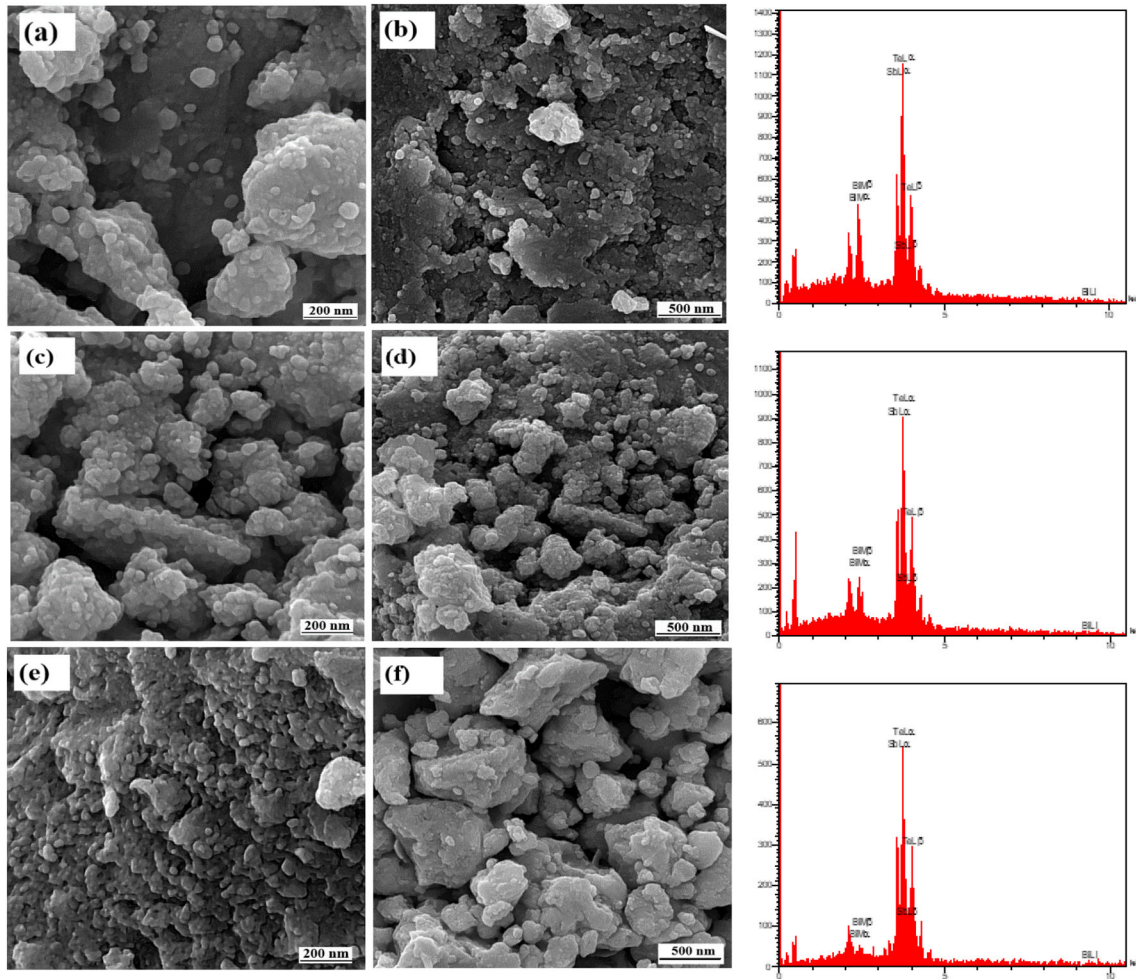


Fig. 3 SEM micrographs and the relevant EDS spectra of: **a, b** $\text{Bi}_{0.2}\text{Sb}_{1.8}\text{Te}_3$ powder, **c, d** $\text{Bi}_{0.3}\text{Sb}_{1.7}\text{Te}_3$ powder, and **e, f** $\text{Bi}_{0.5}\text{Sb}_{1.5}\text{Te}_3$ powder

Table 2 The chemical composition (at.%) of the samples obtained from EDS analyses of powders

Samples	Bi	Sb	Te
$\text{Bi}_{0.2}\text{Sb}_{1.8}\text{Te}_3$	2.60	39.05	58.34
$\text{Bi}_{0.3}\text{Sb}_{1.7}\text{Te}_3$	6.68	34.07	59.25
$\text{Bi}_{0.5}\text{Sb}_{1.5}\text{Te}_3$	10.96	30.22	58.81

The integrated structure confirmed the suitable sintering temperature of 400 °C; however, all samples have sub-micron pores. Definitely, with enhancing sintering temperature, the porosity of the bulk sample decreases due to the increase in the amount of melted particles, although the purity of the ternary compound reduces. Sintering at higher temperatures such as 450 °C was not suitable since

according to the triple diagram for Bi, Sb, and Te, all samples should melt at this temperature. For instance, melting of $\text{Bi}_{0.5}\text{Sb}_{1.5}\text{Te}_3$ compound (with nano-size particle) starts at 413 °C; therefore, at 450 °C, the Te was observed as a liquid phase in the structure. Therefore, 400 °C was selected as the sintering temperature of all samples.

3.3 Electrical conductivity

The electrical conductivity of the samples is demonstrated in Fig. 6. According to Eqs. (1) and (6), some thermoelectric properties such as power factor and the figure of merit demonstrate a proportional relation with electrical conductivity. According to the literature, the reason for the increase in electrical conductivity can be attributed to impurities and defects that cause the electron to scatter. In general,

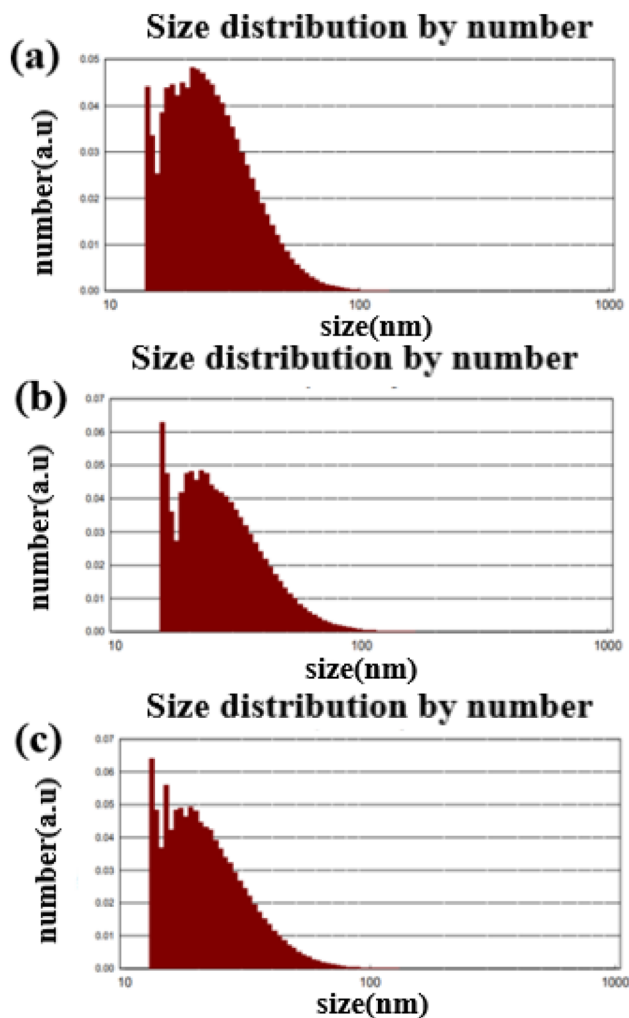


Fig. 4 Grain size distribution in samples: **a** $\text{Bi}_{0.2}\text{Sb}_{1.8}\text{Te}_3$, **b** $\text{Bi}_{0.3}\text{Sb}_{1.7}\text{Te}_3$, and **c** $\text{Bi}_{0.5}\text{Sb}_{1.5}\text{Te}_3$

electrical conductivity (S/cm) is calculated by the following equation [29, 30]:

$$\delta = ne\mu \quad (4)$$

in this case, n and μ are the density the mobility of the carriers, respectively. The results from all the three samples confirm that $\text{Bi}_{0.5}\text{Sb}_{1.5}\text{Te}_3$ presents the best electrical conductivity. This is due to the uniform distribution of fine cavities and the improvement of load-bearing motion. It should also be noted that increasing the amount of Sb to the optimal value in the $\text{Bi}_{2-x}\text{Sb}_x\text{Te}_3$ ($x = 1.5$) sample results in an increase in the electrical conductivity [10].

As mentioned, electrical resistivity depends on two factors: carrier concentration and carrier mobility. The carrier mobility changes by density, grain size, and defects [31]. Therefore, as it was expected, the

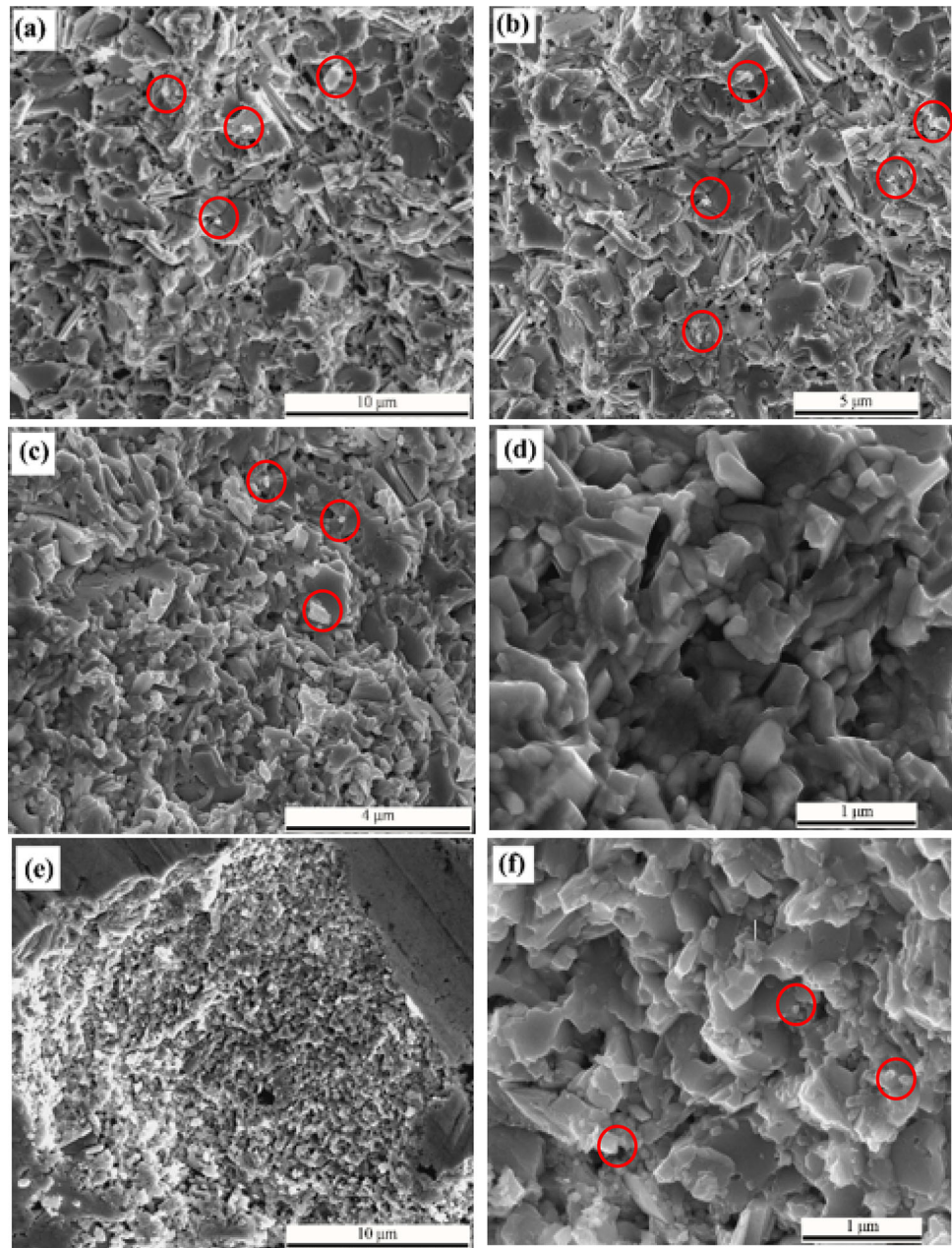
results show that electrical conductivity decreases by an increase of the grain size.

3.4 Seebeck coefficient

The Seebeck results for the three samples (Fig. 7) show that increasing Bi in the chemical composition of the materials has a positive effect on the Seebeck coefficient. The positive Seebeck coefficient demonstrates that all the samples are p-type. In specific, the highest Seebeck coefficient is reported for $\text{Bi}_{0.5}\text{Sb}_{1.5}\text{Te}_3$ at room temperature ($256 \mu\text{V/K}$), while it is $79 \mu\text{V/K}$ for the $\text{Bi}_{0.3}\text{Sb}_{1.5}\text{Te}_3$ compound. As shown in SEM images, the material has integrated structure in which there is a lower carrier concentration, and thus, a lower scattering [32]. Therefore, the carrier movement is easier, and the Seebeck coefficient is higher. In addition, as can be seen in Fig. 7, there is a decreasing trend in the curves from 400 K to 700 K. The Seebeck coefficient obtained in the current study is lower compared with those obtained from some other studies. It can be related to the higher milling time, ratio of ball to powder, and milling rate in the researches [19]. These factors lead to the smaller particle size, decrease of carrier concentration, and the increase of the Seebeck coefficient. A donor-like effect (an interaction between anti-site defects and vacancies) resulted from the heavy plastic deformation during the milling process can be the reason. Li et al. [19] reported that the increase in the milling rate, the ball to powder ratio, and the milling time lead to the formation of extra electron carriers in the lattice and the negative Seebeck coefficient [19]. The study showed that at first, carriers are positive and then with increasing milling time, carriers change to the electron with a negative Seebeck value. However, in the current study, positive Seebeck coefficient was achieved, and it shows that carriers in these semiconductors are holes, instead of electrons. It might be because of the lower energy applied during the synthesis of the compounds using ball-milling process.

Pan et al. [33] ball-milled p-type $\text{Bi}_{0.5}\text{Sb}_{1.5}\text{Te}_3$ and n-type $\text{Bi}_2\text{Te}_{2.7}\text{Se}_{0.3}$ at 450 rpm for 3 h in a purified argon atmosphere with the ball to powder weight ratio of 20:1. The powders were sintered by SPS under uniaxial stress of 50 MPa at 673 K in a vacuum for 5 min. They reported that during the MA process and mechanical deformation, some vacancies are produced and collision of the anti-site defects and

Fig. 5 SEM micrographs of SPSe materials: **a**, **b** $\text{Bi}_{0.2}\text{Sb}_{1.8}\text{Te}_3$, **c**, **d** $\text{Bi}_{0.3}\text{Sb}_{1.7}\text{Te}_3$, and **e**, **f** $\text{Bi}_{0.5}\text{Sb}_{1.5}\text{Te}_3$. Red circles indicate Sb_2O_3 particles (Color figure online)



vacancies results in the decrease of the hole concentration and the increase of the Seebeck coefficient.

Impurities such as Fe entered from milling vessel and balls during the MA process can produce the anti-site defects and thus Seebeck coefficient [32]. According to Fig. 1, there are not such impurities in the synthesized powders, and it may be a reason for the lower Seebeck coefficient in these samples.

Based on Fig. 3, a rise in Bi content from 0.2 to 0.5 at.% results in the reduction of the particle size of the produced powders. Furthermore, it can be noted that the decrease in the size of the produced powders

leads to a decrease in carrier concentration and, of course, a decrease in their scattering. As a result, the movement of the carriers is less disturbed, and the Seebeck coefficient increases [34]. The higher Seebeck coefficient of the $\text{Bi}_{0.5}\text{Sb}_{1.5}\text{Te}_3$ sample is due to the uniform distribution of fine cavities and the improvement of the charge carrier mobility, which can be cited by visual analysis of SEM images. Moreover, it indicates the effect of additives (Bi content) in all samples. According to Fig. 7, increasing the amount of Bi reduces the size of the cavities in the sample and also increases the Seebeck coefficient

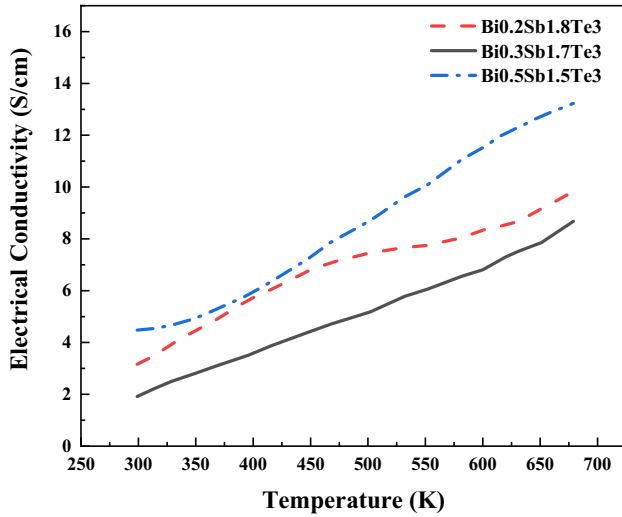


Fig. 6 Electrical conductivity of the SPSed $\text{Bi}_{0.5}\text{Sb}_{1.5}\text{Te}_3$, $\text{Bi}_{0.2}\text{Sb}_{1.8}\text{Te}_3$, and $\text{Bi}_{0.3}\text{Sb}_{1.7}\text{Te}_3$ samples

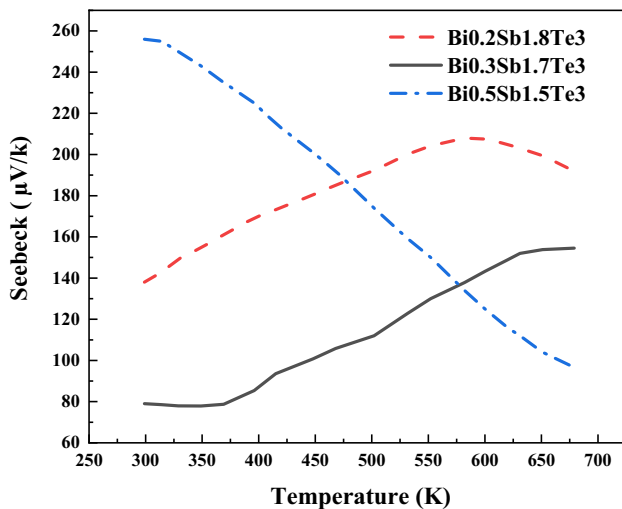


Fig. 7 Seebeck coefficient of $\text{Bi}_{0.5}\text{Sb}_{1.5}\text{Te}_3$, $\text{Bi}_{0.2}\text{Sb}_{1.8}\text{Te}_3$, and $\text{Bi}_{0.3}\text{Sb}_{1.7}\text{Te}_3$ samples SPSed at $400\text{ }^\circ\text{C}$

at ambient temperature which has a positive effect on TE properties.

The Seebeck coefficient variation in the temperature range of 300–700 K can be explained with two factors. The first one is the interaction of the anti-site defects and Te vacancy affecting the carrier concentrations. The second one is the effect of temperature on the mobility of carriers [29]. According to these parameters, the $\text{Bi}_{0.5}\text{Sb}_{1.5}\text{Te}_3$ composition showed the best Seebeck coefficient at room temperature.

3.5 Thermal conductivity

Thermal conductivity was calculated according to the following equation:

$$k = k_{\text{el}} + k_{\text{L}} \quad (5)$$

where k_{el} and k_{L} are the electronic and lattice thermal conductivity, respectively [10]. Figure 8 shows thermal conductivity curves. As can be observed, the thermal conductivity of the $\text{Bi}_{0.5}\text{Sb}_{1.5}\text{Te}_3$ specimen is the lowest at room temperature (0.856 W/m K). Also, due to low k_{el} and k_{L} , it demonstrates the highest phonon scattering in comparison with the other two specimens.

Among other significant factors affecting thermal conductivity, the addition of Bi as a doping agent to the sample $\text{Bi}_{0.5}\text{Sb}_{1.5}\text{Te}_3$ on the one hand increases grain boundaries which in turn, increases phonon scattering. On the other hand, Bi is a heavy element and can decrease lattice fluctuation and, in conclusion, decreases the phonon scattering.

According to Hyoung's study [34], decreasing the grain size causes decreasing of K_{lat} by increasing of phonon scattering. Thus, reduction of the grain size can improve the thermoelectric performance of p-type $\text{Bi}_{0.5}\text{Sb}_{1.5}\text{Te}_3$ alloy by controlling both electronic and thermal transport properties.

In comparison with other results, the thermal conductivity measured in this study was lower. Some sample specifications affecting thermal conductivity

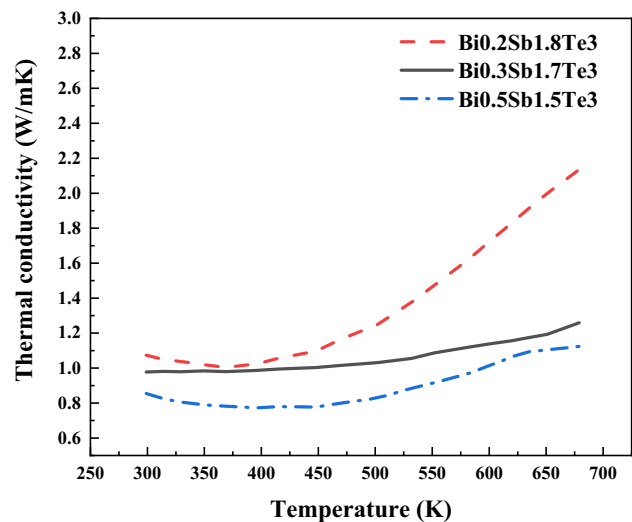


Fig. 8 The temperature-dependent thermal conductivity of $\text{Bi}_{0.5}\text{Sb}_{1.5}\text{Te}_3$, $\text{Bi}_{0.2}\text{Sb}_{1.8}\text{Te}_3$, and $\text{Bi}_{0.3}\text{Sb}_{1.7}\text{Te}_3$ samples SPSed at $400\text{ }^\circ\text{C}$

have been mentioned in the literature such as the amount of impurity, microstructure, and grain size [21]. These parameters are controlled by synthesis parameters.

3.6 Power factor

Figure 9 exhibits the power factor for all the three samples of this study. As can be seen, the power factor is the highest for $\text{Bi}_{0.5}\text{Sb}_{1.5}\text{Te}_3$ at room temperature. Since the power factor is an important parameter influencing the efficiency of thermoelectric properties, the power factor was determined according to the following equation:

$$PF = \delta^2 \alpha \tag{6}$$

in which, δ is the electrical conductivity and α is the Seebeck coefficient. According to the equation, the highest power factor is obtained with the highest Seebeck coefficient and electrical conductivity. As Fig. 9 indicates, the $\text{Bi}_{0.5}\text{Sb}_{1.5}\text{Te}_3$ sample demonstrates the highest power factor among the three samples studied in this research followed by $\text{Bi}_{0.2}\text{Sb}_{1.8}\text{Te}_3$, while $\text{Bi}_{0.3}\text{Sb}_{1.7}\text{Te}_3$ shows the lowest power factor among the samples. In this research, the power factor of $0.29 \mu\text{W}/\text{K}^2 \text{ cm}$ was achieved for the sample $\text{Bi}_{0.5}\text{Sb}_{1.5}\text{Te}_3$ at room temperature. The power factor of these three compositions is resulted from the electrical conductivity and Seebeck coefficient. It means that the trend of power factor coefficient with temperature is affected by the variation of electrical conductivity and Seebeck coefficient. Therefore, the

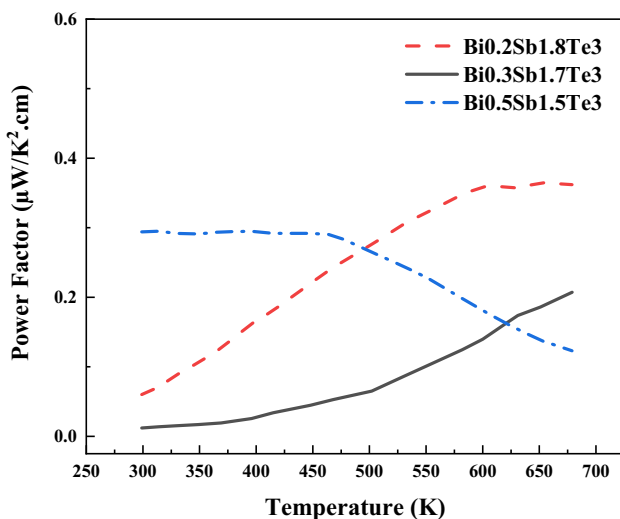


Fig. 9 Power factor of $\text{Bi}_{0.5}\text{Sb}_{1.5}\text{Te}_3$, $\text{Bi}_{0.2}\text{Sb}_{1.8}\text{Te}_3$, and $\text{Bi}_{0.3}\text{Sb}_{1.7}\text{Te}_3$ samples SPSed at $400 \text{ }^\circ\text{C}$

variation of the power factor comes from the concentration and mobility of holes [29].

3.7 Figure of merit

Figure 10 shows the dependency of the figure of merit on temperature for all the three samples synthesized in this study. The figure of merit is a dimensionless parameter that exhibits the productivity of the TE materials and is determined using Eq. (1). Moreover, figure of merit of Bi_2Te_3 -based thermoelectric materials could be improved using the nanostructured materials [35]. The results confirm that the sample with high electrical conductivity, high Seebeck coefficient, and low thermal conductivity, i.e., $\text{Bi}_{0.5}\text{Sb}_{1.5}\text{Te}_3$ sample shows the highest ZT (1.70×10^{-2}) at 468 K, while for $\text{Bi}_{0.3}\text{Sb}_{1.7}\text{Te}_3$ and $\text{Bi}_{0.2}\text{Sb}_{1.8}\text{Te}_3$ samples, this parameter is 0.244×10^{-2} and 0.951×10^{-2} , respectively. Fan et al. [21] fabricated $\text{Bi}_{0.5}\text{Sb}_{1.5}\text{Te}_3$ compounds using hot pressing at 300, 400, 450, and $500 \text{ }^\circ\text{C}$. They found that ZT increases with increasing sintering temperature. The results showed that the sample sintered at $500 \text{ }^\circ\text{C}$ presents the maximum figure of merit of 2.84×10^{-3} at room temperature which is lower in comparison with the figure of merit of the specimen synthesized in the current study.

Table 3 summarizes the thermoelectric properties of the synthesized compounds at 468 K, at which the higher ZT value has been obtained. In this research, $\text{Bi}_{0.5}\text{Sb}_{1.5}\text{Te}_3$ was compared with other TE materials such as $\text{Bi}_{0.2}\text{Sb}_{1.8}\text{Te}_3$ and $\text{Bi}_{0.3}\text{Sb}_{1.7}\text{Te}_3$ and exhibited better thermoelectric properties, including higher

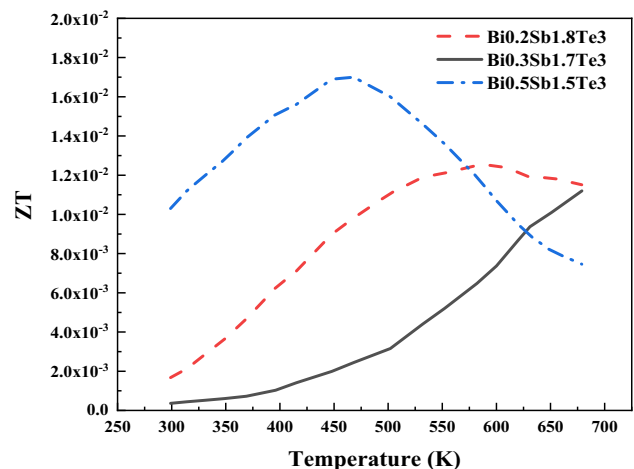


Fig. 10 Figure of merit of $\text{Bi}_{0.5}\text{Sb}_{1.5}\text{Te}_3$, $\text{Bi}_{0.2}\text{Sb}_{1.8}\text{Te}_3$, and $\text{Bi}_{0.3}\text{Sb}_{1.7}\text{Te}_3$ samples SPSed at $400 \text{ }^\circ\text{C}$

Table 3 Thermoelectric properties of $\text{Bi}_{2-x}\text{Sb}_x\text{Te}_3$ samples: total thermal conductivity (k_{tot}), Seebeck coefficient (S), electrical conductivity (σ), power factor (PF), and the figure of merit (ZT) at room temperature

Sample	T (K)	K_{tot} (W/mK)	S ($\mu\text{V/K}$)	σ (S/cm)	PF ($\mu\text{W/K}^2 \text{ cm}$)	ZT
$\text{Bi}_{0.2}\text{Sb}_{1.8}\text{Te}_3$	299	1.073	138	3.16	0.0601	1.67×10^{-2}
$\text{Bi}_{0.3}\text{Sb}_{1.7}\text{Te}_3$	299	0.977	79	1.91	0.011	3.65×10^{-2}
$\text{Bi}_{0.5}\text{Sb}_{1.5}\text{Te}_3$	299	0.856	256	4.48	0.294	1.03×10^{-2}

electrical conductivity and lower thermal conductivity. Finally, the $\text{Bi}_{0.5}\text{Sb}_{1.5}\text{Te}_3$ compound demonstrated the highest figure of merit.

4 Conclusions

In this study, three p-type thermoelectric compounds, i.e., $\text{Bi}_{2-x}\text{Sb}_x\text{Te}_3$ with $x = (1.2, 1.3, 1.5)$, were fabricated using mechanical alloying and spark plasma sintering (SPS). The microstructure and thermoelectric properties of the samples were analyzed and the following results were achieved:

1. A 6-h milling led to the formation of single phases of $\text{Bi}_{0.5}\text{Sb}_{1.5}\text{Te}_3$ and $\text{Bi}_{0.2}\text{Sb}_{1.8}\text{Te}_3$ rhombohedral structures; however, some impurities were seen along with the formation of the $\text{Bi}_{0.3}\text{Sb}_{1.7}\text{Te}_3$ single phase.
2. SEM images showed micropores with sizes of less than 50 microns uniformly distributed in the structure of $\text{Bi}_{0.5}\text{Sb}_{1.5}\text{Te}_3$ TE material.
3. Increasing the Bi content from 0.2 to 0.5 at.% resulted in a higher amount of power factor ($0.294 \mu\text{W/K}^2 \text{ cm}^{-1}$), lower thermal conductivity (0.856 W/mK) and an increase in the electrical conductivity (0.854 S/cm) at room temperature.
4. A comparison of the three synthesized compounds confirmed that $\text{Bi}_{0.5}\text{Sb}_{1.5}\text{Te}_3$ material with the highest homogeneity and the lowest grain size demonstrates the highest ZT (1.70×10^{-2}) at 468 K.

Acknowledgements

The authors appreciate the support from Ferdowsi University of Mashhad (FUM) under the research scheme No. 3/48155. Moreover, assistance of Prof. Muhammet S. Toprak and Mr. Bejan Hamawandi, from the Department of Applied Physics, KTH Royal

Institute of Technology, Stockholm, Sweden, and Sedat Ballikaya from the Department of Physics, Istanbul University, Istanbul, Turkey are widely acknowledged.

References

1. D.G. Bulusu, Walker, Review of electronic transport models for thermoelectric materials. *Superlattices Microstruct.* **44**, 1–36 (2008). <https://doi.org/10.1016/j.spmi.2008.02.008>
2. C. Van der Rest, V. Dupont, J.-P. Erauw, P.J. Jacques, On the reactive sintering of Heusler Fe_2VAI -based thermoelectric compounds. *Intermetallics.* **125**, 106890 (2020). <https://doi.org/10.1016/j.intermet.2020.106890>
3. Y. Sb, G. Zhang, J. Xu, F. Mi, Z. Han, C. Wang, Ge, Hydrothermal synthesis and thermoelectric properties of nanostructures. *Mater. Res. Bull.* **46**, 760–764 (2011). <https://doi.org/10.1016/j.materresbull.2010.11.024>
4. S. Bano, A. Kumar, B. Govind, A.H. Khan, A. Ashok, D.K. Misra, Room temperature Bi_2Te_3 -based thermoelectric materials with high performance. *J. Mater. Sci. Mater. Electron.* **31**, 8607–8617 (2020). <https://doi.org/10.1007/s10854-020-03396-6>
5. P. Dharmiaiah, H. Kim, C. Lee, S. Hong, Influence of powder size on thermoelectric properties of p-type 25% Bi_2Te_3 -75% Sb_2Te_3 alloys fabricated using gas atomization and spark-plasma sintering. *J. Alloys Compd.* (2016). <https://doi.org/10.1016/j.jallcom.2016.05.340>
6. H. Zhang, F. Ye, Y. Hu, J. Liu, Y. Zhang, Y. Wu, Z. Hu, The investigation of thermal properties on multilayer $\text{Sb}_2\text{Te}_3/\text{Au}$ thermoelectric material system with ultra-thin Au interlayers. *Superlattices Microstruct.* **89**, 312–318 (2016). <https://doi.org/10.1016/j.spmi.2015.11.022>
7. Y. Saberi, S.A. Sajjadi, H. Mansouri, Comparison of characteristics of Bi_2Te_3 and $\text{Bi}_2\text{Te}_{2.7}\text{Se}_{0.3}$ thermoelectric materials synthesized by hydrothermal process. *J. Mater. Sci. Mater. Electron.* (2020). <https://doi.org/10.1007/s10854-020-04435-y>
8. P. Dharmiaiah, S.J. Hong, Hydrothermal method for the synthesis of Sb_2Te_3 , and $\text{Bi}_{0.5}\text{Sb}_{1.5}\text{Te}_3$ nanoplates and their

- thermoelectric properties. *Int. J. Appl. Ceram. Technol.* **15**, 132–139 (2018). <https://doi.org/10.1111/ijac.12762>
9. G.S. Hegde, A.N. Prabhu, R.Y. Huang, Y.K. Kuo, Reduction in thermal conductivity and electrical resistivity of indium and tellurium co-doped bismuth selenide thermoelectric system. *J. Mater. Sci. Mater. Electron.* (2020). <https://doi.org/10.1007/s10854-020-04383-7>
 10. L. Han, S.H. Spangsdorf, N.V. Nong, L.T. Hung, Y.B. Zhang, H.N. Pham, Y.Z. Chen, A. Roch, L. Stepien, N. Pryds, Effects of spark plasma sintering conditions on the anisotropic thermoelectric properties of bismuth antimony telluride. *RSC Adv.* **6**, 59565–59573 (2016). <https://doi.org/10.1039/c6ra06688g>
 11. Y. Dou, X. Yan, Y. Du, J. Xu, D. Li, Thermoelectric properties of $\text{Bi}_{0.4}\text{Sb}_{1.6}\text{Te}_3$ -based composites with silicon nano-inclusions. *J. Mater. Sci. Mater. Electron.* **31**, 4808–4814 (2020). <https://doi.org/10.1007/s10854-020-03042-1>
 12. W. Wang, B. Poudel, J. Yang, D.Z. Wang, Z.F. Ren, High-yield synthesis of single-crystalline antimony telluride hexagonal nanoplates using a solvothermal approach. *J Am Chem Soc* **127**, 13792–13793 (2005)
 13. S. Fan, J. Zhao, J. Guo, Q. Yan, J. Ma, H.H. Hng, P-type $\text{Bi}_{0.4}\text{Sb}_{1.6}\text{Te}_3$ nanocomposites with enhanced figure of merit. *Appl. Phys. Lett.* **96**, 2010–2013 (2010). <https://doi.org/10.1063/1.3427427>
 14. A. Kadhim, A. Hmood, H.A. Hassan, Physical properties of $\text{Bi}_2(\text{Te, Se})_3$ and $\text{Bi}_2\text{Se}_{1.2}\text{Te}_{1.8}$ prepared sing solid-state microwave synthesis. *Mater. Lett.* **65**, 3105–3108 (2011). <https://doi.org/10.1016/j.matlet.2011.06.069>
 15. B. Poudel, Q. Hao, Y. Ma, Y. Lan, A. Minnich, B. Yu, X. Yan, D. Wang, A. Muto, D. Vashaee, X. Chen, J. Liu, M.S. Dresselhaus, G. Chen, Z. Ren, High-thermoelectric performance of nanostructured bismuth antimony telluride bulk alloys. *Science* (2008). <https://doi.org/10.1126/science.1155140>
 16. B. Madavali, H.S. Kim, C.H. Lee, D. Soo Kim, S.J. Hong, High thermoelectric figure of merit in p-type $\text{Bi}_2\text{Te}_3)_x - (\text{Sb}_2\text{Te}_3)_{1-x}$ alloys made from element-mechanical alloying and spark plasma sintering. *J. Electron. Mater.* **48**, 416–424 (2019). <https://doi.org/10.1007/s11664-018-6706-7>
 17. M.G. Kanatzidis, S.D. Mahanti, and T.P. Hogan. Chemistry, physics, and materials science of thermoelectric materials: beyond bismuth telluride. *Fundamental Materials Research*. ISBN 978-1-4613-4872-6 ISBN 978-1-4419-9278-9 (eBook). <https://doi.org/10.1007/978-1-4419-9278-9>.
 18. D.C. Cho, S.Y. Kim, C.H. Lim, W.S. Cho, H. Lee, S.Y. Shin, Z.A. Munir, Thermoelectric properties of P-Type $\text{Bi}_{0.5}\text{Sb}_{1.5}\text{Te}_3$ compounds prepared by spark plasma sintering method. *J. Ceram. Trans.* (2006). <https://doi.org/10.1002/9780470082751.ch25>
 19. H. Li, H. Jing, Y. Han, G. Lu, L. Xu, Intermetallics Effects of mechanical alloying process and sintering methods on the microstructure and thermoelectric properties of bulk $\text{Bi}_{0.5}\text{Sb}_{1.5}\text{Te}_3$ alloy. *Intermetallics.* **43**, 16–23 (2013). <https://doi.org/10.1016/j.intermet.2013.07.007>
 20. C. Chen, D. Liu, B. Zhang, J. Li, Enhanced thermoelectric properties obtained by compositional optimization in p-type $\text{Bi}_x\text{Sb}_{2-x}\text{Te}_3$ fabricated by mechanical alloying and spark plasma sintering. **40**(5), 942–947 (2011). <https://doi.org/10.1007/s11664-010-1463-2>
 21. X.A. Fan, J.Y. Yang, R.G. Chen, W. Zhu, S.Q. Bao, Phase transformation and thermoelectric properties of p-type $(\text{Bi}_{2-x}\text{Te}_3)_{0.25}(\text{Sb}_2\text{Te}_3)_{0.75}$ prepared by mechanical alloying and hot pressing. *Mater. Sci. Eng. A.* **438–440**, 190–193 (2006). <https://doi.org/10.1016/j.msea.2005.12.055>
 22. M. Kitamura, K. Hirota, K. Hasezaki, Relationships between thermoelectric properties and milling rotational speed on $\text{Bi}_{0.3}\text{Sb}_{1.7}\text{Te}_{3.0}$ thermoelectric materials. *Mater. Trans.* **59**, 1225–1232 (2018). <https://doi.org/10.2320/matertrans.MF201703>
 23. Z. Chen, M.Y. Lin, G.D. Xu, S. Chen, J.H. Zhang, M.M. Wang, Hydrothermal synthesized nanostructure Bi-Sb-Te thermoelectric materials. *J. Alloys Compd.* **588**, 384–387 (2014). <https://doi.org/10.1016/j.jallcom.2013.11.065>
 24. S.J. Madavali, Hong, Enhanced thermoelectric properties of p-type $\text{Bi}_{0.5}\text{Sb}_{1.5}\text{Te}_3$ thermoelectric materials by mechanical alloying and spark plasma sintering. *J. Electron. Mater.* **45**, 6059–6066 (2016). <https://doi.org/10.1007/s11664-016-5011-6>
 25. M. Likha, P. Dharmiah, B. Madavali, C. Lee, D. Shin, G. Song, K. Lee, S. Hong, Intermetallics Oxide formation mechanism and its effect on the microstructure and thermoelectric properties of p-type $\text{Bi}_{0.5}\text{Sb}_{1.5}\text{Te}_3$ alloys. *Intermetallics.* **103**, 23–32 (2018). <https://doi.org/10.1016/j.intermet.2018.09.015>
 26. L. Liao, C. Wu, L. Liao, Wu, Enhancement of carrier transport properties of $\text{Bi}_x\text{Sb}_{2-x}\text{Te}_3$ compounds by electrical sintering process Enhancement of carrier transport properties of $\text{Bi}_x\text{Sb}_{2-x}\text{Te}_3$ compounds by electrical sintering process. *Appl. Phys. Lett.* (2014). <https://doi.org/10.1063/1.3196315>
 27. A. Pakdel, Q. Guo, V. Nicolosi, T. Mori, Enhanced thermoelectric performance of Bi-Sb-Te/ Sb_2O_3 nanocomposites by energy filtering effect. *J. Mater. Chem. A.* **6**, 21341–21349 (2018). <https://doi.org/10.1039/c8ta08238c>
 28. C. Robinson, Preparation of bismuth telluride based thermoelectric nanomaterials via low-energy ball milling and their property characterizations. *Open Access Theses.* **601** (2015). https://docs.lib.purdue.edu/open_access_theses/601
 29. S. Lim, J. Kim, B. Kwon, S. Keun, H. Park, K. Lee, J. Min, W. Jun, D. Kim, D. Hyun, J. Kim, S. Baek, Effect of spark

- plasma sintering conditions on the thermoelectric. *J. Alloys Compd.* **678**, 396–402 (2016). <https://doi.org/10.1016/j.jallcom.2016.03.284>
30. W.D. Callister, D.G. Rethwisch, *Materials Science and Engineering* (John Wiley and Sons, Inc, London, 2018), p 992. ISBN: 978-1-119-40549-8
 31. S.J. Hong, K.S. Hwang, J.W. Byeon, M.K. Lee, C.K. Rhee, B.S. Chun, The effect of powder size on thermoelectric properties of 95%Bi₂Te₃-5%Bi₂Se₃ alloy. *Solid State Phenom.* **119**, 271–274 (2007)
 32. D.M. Lee, C.H. Lim, S.Y. Shin, D.C. Cho, C.H. Lee, Thermoelectric properties of p-type Bi_{0.5}Sb_{1.5}Te₃ compounds fabricated by spark plasma sintering. *J. Electroceram.* **17**, 879–883 (2006). <https://doi.org/10.1007/s10832-006-6807-1>
 33. Y. Pan, T.R. Wei, Q. Cao, J.F. Li, Mechanically enhanced p- and n-type Bi₂Te₃-based thermoelectric materials reprocessed from commercial ingots by ball milling and spark plasma sintering. *Mater. Sci. Eng. B Solid-State Mater. Adv. Technol.* **197**, 75–81 (2015). <https://doi.org/10.1016/j.mseb.2015.03.011>
 34. K. Hyoung, W. Ho, H. Kim, K. Lee, J. Wook, J. Yoo, J. Kim, S. Wng, S. Kim, Scripta Materialia Synergetic effect of grain size reduction on electronic and thermal transport properties by selectively-suppressed minority carrier mobility and enhanced boundary scattering in Bi_{0.5}Sb_{1.5}Te₃ alloys, *Scr. Mater.* **160**, 15–19 (2019). <https://doi.org/10.1016/j.scriptamat.2018.09.038>
 35. N. Mntungwa, P.V.S.R. Rajasekhar, K. Ramasamy, N. Revaprasadu, A simple route to Bi₂Se₃ and Bi₂Te₃ nanocrystals, *Superlattices Microstruct.* **69**, 226–230 (2014). <https://doi.org/10.1016/j.spmi.2014.02.021>
- Publisher's Note** Springer Nature remains neutral with regard to jurisdictional claims in published maps and institutional affiliations.

Terms and Conditions

Springer Nature journal content, brought to you courtesy of Springer Nature Customer Service Center GmbH (“Springer Nature”).

Springer Nature supports a reasonable amount of sharing of research papers by authors, subscribers and authorised users (“Users”), for small-scale personal, non-commercial use provided that all copyright, trade and service marks and other proprietary notices are maintained. By accessing, sharing, receiving or otherwise using the Springer Nature journal content you agree to these terms of use (“Terms”). For these purposes, Springer Nature considers academic use (by researchers and students) to be non-commercial.

These Terms are supplementary and will apply in addition to any applicable website terms and conditions, a relevant site licence or a personal subscription. These Terms will prevail over any conflict or ambiguity with regards to the relevant terms, a site licence or a personal subscription (to the extent of the conflict or ambiguity only). For Creative Commons-licensed articles, the terms of the Creative Commons license used will apply.

We collect and use personal data to provide access to the Springer Nature journal content. We may also use these personal data internally within ResearchGate and Springer Nature and as agreed share it, in an anonymised way, for purposes of tracking, analysis and reporting. We will not otherwise disclose your personal data outside the ResearchGate or the Springer Nature group of companies unless we have your permission as detailed in the Privacy Policy.

While Users may use the Springer Nature journal content for small scale, personal non-commercial use, it is important to note that Users may not:

1. use such content for the purpose of providing other users with access on a regular or large scale basis or as a means to circumvent access control;
2. use such content where to do so would be considered a criminal or statutory offence in any jurisdiction, or gives rise to civil liability, or is otherwise unlawful;
3. falsely or misleadingly imply or suggest endorsement, approval, sponsorship, or association unless explicitly agreed to by Springer Nature in writing;
4. use bots or other automated methods to access the content or redirect messages
5. override any security feature or exclusionary protocol; or
6. share the content in order to create substitute for Springer Nature products or services or a systematic database of Springer Nature journal content.

In line with the restriction against commercial use, Springer Nature does not permit the creation of a product or service that creates revenue, royalties, rent or income from our content or its inclusion as part of a paid for service or for other commercial gain. Springer Nature journal content cannot be used for inter-library loans and librarians may not upload Springer Nature journal content on a large scale into their, or any other, institutional repository.

These terms of use are reviewed regularly and may be amended at any time. Springer Nature is not obligated to publish any information or content on this website and may remove it or features or functionality at our sole discretion, at any time with or without notice. Springer Nature may revoke this licence to you at any time and remove access to any copies of the Springer Nature journal content which have been saved.

To the fullest extent permitted by law, Springer Nature makes no warranties, representations or guarantees to Users, either express or implied with respect to the Springer nature journal content and all parties disclaim and waive any implied warranties or warranties imposed by law, including merchantability or fitness for any particular purpose.

Please note that these rights do not automatically extend to content, data or other material published by Springer Nature that may be licensed from third parties.

If you would like to use or distribute our Springer Nature journal content to a wider audience or on a regular basis or in any other manner not expressly permitted by these Terms, please contact Springer Nature at

onlineservice@springernature.com